Cement and Concrete Composites 103 (2019) 149–159

Contents lists available at ScienceDirect

Cement and Concrete Composites

journal homepage: www.elsevier.com/locate/cemconcomp

Examining the effects of microencapsulated phase change materials on early-age temperature evolutions in realistic pavement geometries

Zhenyu She[a], Zhenhua Wei[b], Benjamin A. Young[a], Gabriel Falzone[b], Narayanan Neithalath[c], Gaurav Sant[b,d,**], Laurent Pilon[a,d,*]

[a] Department of Mechanical and Aerospace Engineering, University of California, Los Angeles, USA
[b] Department of Civil and Environmental Engineering, University of California, Los Angeles, USA
[c] School of Sustainable Engineering and the Built Environment, Arizona State University, USA
[d] California NanoSystems Institute (CNSI), University of California, Los Angeles, USA

ARTICLE INFO

Keywords:
Microencapsulated phase change materials
Concrete pavement
Early-age cracking
Water-reducing admixture
Cement hydration

ABSTRACT

This study examines experimentally and numerically the effects of microencapsulated phase change material (PCM) additions on temperature rise and cool-down rate, and the associated impact on reducing the risk of thermal cracking in concrete pavements. Specimens representative of a realistic pavement geometry were exposed to diurnal temperature cycling at early ages while internal temperature evolutions were monitored. In spite of the fact that the lower thermal conductivity of the PCM inhibited heat dissipation, the results showed the presence of PCMs can reduce considerably the temperature rise and cool-down rate in the first 24 h following placement provided the PCM melting temperature is chosen suitably. A transient one-dimensional thermal model of a pavement section suitably captured experimental temperature evolutions and thereby offers the ability to inform the design of concrete pavements containing PCMs that feature early-age thermal cracking resistance.

1. Introduction

The exothermic nature of cement-water ("hydration") reactions results in temperature rise within concrete sections. The extent of temperature rise depends on the section geometry and the environmental conditions, and results in the development of temperature gradients within restrained sections, e.g., concrete pavements [1–3]. Excessive temperature rise, and the development of such thermal gradients are a leading cause of thermal cracking in concrete pavements; more so when multiple deformation processes, e.g., autogenous, drying and thermal deformations may superimpose [1]. To mitigate thermal cracking, several methods have been developed including (i) reducing the cement content, i.e., by replacing cement with mineral admixtures (e.g., fly ash, silica fume, and slag) [4], (ii) changing the time of concrete placement (e.g., night placement) [2], and (iii) using ice as a sink for the heat released during hydration [5].

The dosage of microencapsulated phase change materials (PCMs) into concrete has been recently proposed as a means to reduce temperature rise of concrete at early ages [6–9]. PCMs are thermal energy storage materials that can store latent heat associated with reversible melting and solidification processes [10,11]. In order to avoid leakage, and to isolate the PCM from the alkaline cementitious environment, PCMs are often encapsulated in a polymeric casing [12,13]. As heat is released by cement hydration, it is absorbed and stored in the form of latent heat of fusion in the microencapsulated PCMs. This reduces the maximum temperature that can be achieved, the rate of temperature change (i.e., both heating and cooling), and the temperature gradient that develops in a concrete section [3,14]. Taken together, these effects act to diminish the driving forces of thermal cracking in restrained concrete sections.

Šavija et al. [15] developed numerical models to predict the temperature and stress distribution in wall-on-slab systems. They confirmed that the addition of microencapsulated PCMs reduces temperature rise and stress development in concrete structures. Arora et al. [14] conducted numerical simulations to study both the early- and later-age thermal response of concrete pavements containing microencapsulated PCMs. They identified that PCMs reduce both the peak hydration temperature and heating/cooling rates when they are incorporated into concrete pavements. Furthermore, simulations on mature pavements indicated temperature and curling stress reductions when appropriate

* Corresponding author. Engineering IV, 420 Westwood Plaza, Los Angeles, CA, 90095-1597, USA.
** Corresponding author. Department of Civil and Environmental Engineering, University of California, Los Angeles, USA.
E-mail addresses: gsant@ucla.edu (G. Sant), pilon@seas.ucla.edu (L. Pilon).

https://doi.org/10.1016/j.cemconcomp.2019.04.002
Received 13 July 2018; Received in revised form 11 February 2019; Accepted 1 April 2019
Available online 24 April 2019
0958-9465/

Nomenclature

C_c	cement content, kg/m^3
c_p	specific heat, J/kg K
f	objective function
h	convective heat transfer coefficient, W/m^2 K
h_{sf}	latent heat of fusion, kJ/kg
k	thermal conductivity, W/m K
L_c	height of PCM-mortar composite slab, m
L_s	steel plate thickness, m
$\dot{q}(t)$	volumetric heat generation rate, W/m^3
$\dot{q}_g(t)$	heat generation rate per unit mass of cement, W/kg
$Q(t)$	cumulative volumetric heat generated, J/m^3
$Q_g(t)$	cumulative heat generated per unit mass of cement, J per kg
t	time, s or h
t_{eq}	equivalent time, s or h
$T(x, t)$	temperature at location x and time t, ˚C
T_{pc}	PCM phase change temperature, ˚C
ΔT_{pc}	PCM phase change temperature window, ˚C
T_{ref}	reference temperature, ˚C
T_{max}	maximum temperature of composite slab, ˚C
w/c	water/cement ratio
x	distance from the bottom of composite slab, m

Greek symbols

ρ	density, kg/m^3
ϕ_j	volume fraction of material ”j” in composite
τ	oscillation period, h

Subscripts

c	refers to PCM-mortar composite slab
eff	refers to effective properties
m	refers to cement paste matrix in composite
pcm	refers to phase change material
q	refers to quartz sand
s	refers to steel plate
w	refers to water in the water bath
∞	refers to air in the chamber

PCMs were used that, in turn, resulted in reductions in fatigue damage [14–16]. More recently, Young et al. [3] highlighted that the PCM's phase change temperature needs to be matched to the environmental conditions to ensure adequate reduction in temperature rise. Finally, while Fernandes et al. [7] experimentally demonstrated the ability of PCMs to reduce temperature rise, and the stress developed, their study examined section sizes substantially smaller than a typical pavement section. As such, to date, few if any studies have examined the ability of PCMs to reduce the extent of temperature rise, and the rate of temperature change in realistic-sized pavement sections exposed to diurnal temperature cycling.

This study aims to quantify temperature evolutions and the rates of temperature change within concrete pavement sections containing microencapsulated PCMs at early ages. It also aims to develop a validated 1D transient thermal model that can accurately predict temperature development in realistic-sized (concrete) pavement sections. These outcomes provide the ability to estimate the risk of thermal cracking in concrete pavements as a function of the binder characteristics, environmental conditions, *a priori*. They can also prescribe methods, based on the use of PCMs, to mitigate the risk of thermal cracking.

2. Background

2.1. Thermal modeling of PCM-mortar composites

The PCM-mortar composite considered herein was a heterogeneous composite material consisting of spherical PCM microcapsules randomly distributed in a mortar matrix. It has been demonstrated that its transient thermal behavior is equivalent to that of a homogeneous material with ”effective” thermal properties [17,18]. The effective thermal conductivity k_{eff} of such composites can be predicted by the Felske's model as described elsewhere [17,19,20]. The effective volumetric heat capacity of the PCM-mortar composite is given by the volume-weighted average of the heat capacity of the different constituent materials [18],

$$(\rho c_p)_{eff}(T) = \phi_m(\rho c_p)_m + \phi_q(\rho c_p)_q + (1 - \phi_m - \phi_q)(\rho c_p)_{pcm}. \quad (1)$$

Here, ϕ_m and ϕ_q are the volume fractions of cement paste and quartz sand, respectively, while $(\rho c_p)_m$, $(\rho c_p)_q$, and $(\rho c_p)_{pcm}$ are the volumetric heat capacities of the cement paste, quartz sand, and PCM, respectively. The specific heat capacity of PCM $c_{p,pcm}(T)$ can be described as a rectangular step function of temperature according to the effective heat capacity method [4],

$$c_{p,pcm}(T) = \begin{cases} c_{p,pcm,s} & T < T_{pc} - \Delta T_{pc}/2 \\ c_{p,pcm,s} + \frac{h_{sf}}{\Delta T_{pc}} & T_{pc} - \Delta T_{pc}/2 \le T \le T_{pc} + \Delta T_{pc}/2 \\ c_{p,pcm,l} & T > T_{pc} + \Delta T_{pc}/2 \end{cases} \quad (2)$$

where $c_{p,pcm,s}$ and $c_{p,pcm,l}$ are the specific heat capacity of the PCM in the solid and liquid phases, respectively, h_{sf} is the latent heat of fusion (in J/kg), T_{pc} is the PCM melting temperature, and ΔT_{pc} is the melting temperature window, over which phase change occurs. The effective heat capacity method has been shown to accurately predict temperature evolutions of PCM-mortar composites similar to those obtained using (i) experimentally measured $c_{p,pcm}(T)$ and (ii) its Gaussian fit which is more representative of behavior observed in realistic systems [21].

2.2. Heat generation rate in early-age PCM-mortar composites

Modeling the heat generation rate of hydration reactions is essential for predicting temperature evolution in concrete. The equivalent age method can be used to describe the progress of hydration reactions in cementitious materials [3,22,23]. The equivalent age $t_{eq}(x, t)$ can be expressed as a function of time and temperature history at a given location, i.e. [24],

$$t_{eq}(x, t) = \int_0^t \exp\left[-\frac{E_a}{R}\left(\frac{1}{T_c(x, t)} - \frac{1}{T_{ref}}\right)\right] dt \quad (3)$$

where E_a (in kJ/mol) is the activation energy, $R = 8.314$ J/mol K is the ideal gas constant, T_{ref} is the reference temperature, in K. Then, the local heat generation rate $\dot{q}(x, t)$ (in W/m^3) during the hydration process can be expressed as a function of equivalent age t_{eq} [3,22],

$$\dot{q}(x, t) = \frac{dQ(t_{eq})}{dt_{eq}} \times \frac{dt_{eq}}{dt} = \dot{q}(t_{eq}) \times \exp\left[-\frac{E_a}{R}\left(\frac{1}{T_c(x, t)} - \frac{1}{T_{ref}}\right)\right] \quad (4)$$

where $Q(t_{eq})$ is the cumulative volumetric thermal energy released as a function of equivalent age, and $\dot{q}(t_{eq})$ is the heat generation rate as a function of equivalent age. Both of these quantities are determined simultaneously from isothermal calorimetry measurements at a given reference temperature T_{ref} [3].

3. Materials and methods

3.1. Mixture proportions for PCM-mortar composites

Four cementitious specimens (38 cm × 38 cm × 38 cm) were prepared with the following mixture proportions: (1) a plain mortar consisting of 45 vol% cement paste and 55 vol% quartz inclusions, (2) a microencapsulated PCM-mortar composite consisting of 45 vol% cement paste, 45 vol% quartz, and 10 vol% MPCM24D (Microtek Laboratories, Inc.) with melting temperature $T_{pc} \simeq 24^{\circ}C$ and latent heat of fusion $h_{sf} = 160$ kJ/kg, (3) a microencapsulated PCM-mortar composite consisting of 45 vol% cement paste, 45 vol% quartz, and 10 vol% PCM35CP (Encapsys, LLC) with melting temperature $T_{pc} \simeq 35^{\circ}C$ and latent heat of fusion $h_{sf} = 187$ kJ/kg and (4) a microencapsulated PCM-mortar composite consisting of 45 vol% cement paste, 35 vol% quartz, and 20 vol% PCM35CP. The microencapsulated PCM consisted of a paraffin-based core material encased in a melamine-formaldehyde (MF) shell. The cement paste was mixed using ASTM C150 [25] compliant Type I/II ordinary Portland cement (OPC) and deionized water with a water-cement ratio of 0.45 (mass basis) in accordance with ASTM C192 [26]. ASTM C778 [27] compliant graded quartz sand and microencapsulated PCM were used as inclusions within the cement mortar. Additionally, a water-reducing admixture (WRA, MasterGlenium 7500, BASF Corporation) was added at a dosage level suitable to ensure similar workability across all mortar formulations. As such, the WRA was added at dosage of (i) 0.8% by mass of cement for Composition 1, (ii) 1.5% by mass of cement for Compositions 2 and 3, and (iii) 2.0% by mass of cement for Composition 4. Also, a viscosity-modifying admixture (MasterMatrix VMA 450, BASF Corporation) was added at 260 ml/100 kg of cement to minimize segregation of inclusions and to maintain a homogeneous distribution of PCM microcapsules and quartz sand inclusions in all mortars. Table 1 summarizes the mixture proportions for these four PCM-mortar composite specimens. Finally, an evaporation retardant and finishing aid for concrete (MasterKure 111WB, BASF Corporation) was sprayed onto the top surface of the composite samples immediately after their placement to reduce moistures loss by evaporation.

3.2. Isothermal calorimetry

To obtain the heat generation term $\dot{q}(t_{eq})$ given by Equation (4), an isothermal calorimeter (Tam Air, TA Instruments) was used to measure the volumetric thermal energy $Q(t_{eq})$ released and the corresponding heat generation rate $\dot{q}(t_{eq})$ within PCM-mortar composite specimens due to cement hydration for different mixture proportions. The measurements were performed for 7 days as described in ASTM C1702 [28]. The testing temperature of the isothermal calorimeter was set to the same reference temperature $T_{ref} = 298$ K. Reference specimens of DI water were prepared with a total thermal capacity equivalent to that of the cementitious composites and used to measure the baseline heat flow signal. The baseline signal was subtracted from the measured heat flow of the cementitious composites. All mixture ingredients were conditioned to the testing temperature before mixing. Immediately after mixing, approximately 10 g of each sample was loaded into a 20 mL glass ampoule, sealed, and placed into the calorimeter. Table 2 summarizes the compositions of six different mortar samples synthesized to measure $\dot{q}(t_{eq})$ by isothermal calorimetry. The WRA used in these calorimetric experiments was the same as in the four cementitious specimens (i.e., MasterGlenium 7500, BASF Corporation), classified as Type A or Type F WRA in compliance with ASTM C494/C494M [29].

Table 2
Mixture proportions of the six PCM-mortar composite samples used to measure heat generation rate by isothermal calorimetry.

Sample	Cement paste (vol. %)	ASTM quartz sand (vol.%)	MPCM24D (vol.%)	Water-cement ratio (%)	WRA (wt.% cement)
1	100	0	0	45	0
2	100	0	0	45	0.8
3	90	0	10	45	0
4	90	0	10	45	0.8
5	90	10	0	45	0
6	90	10	0	45	0.8

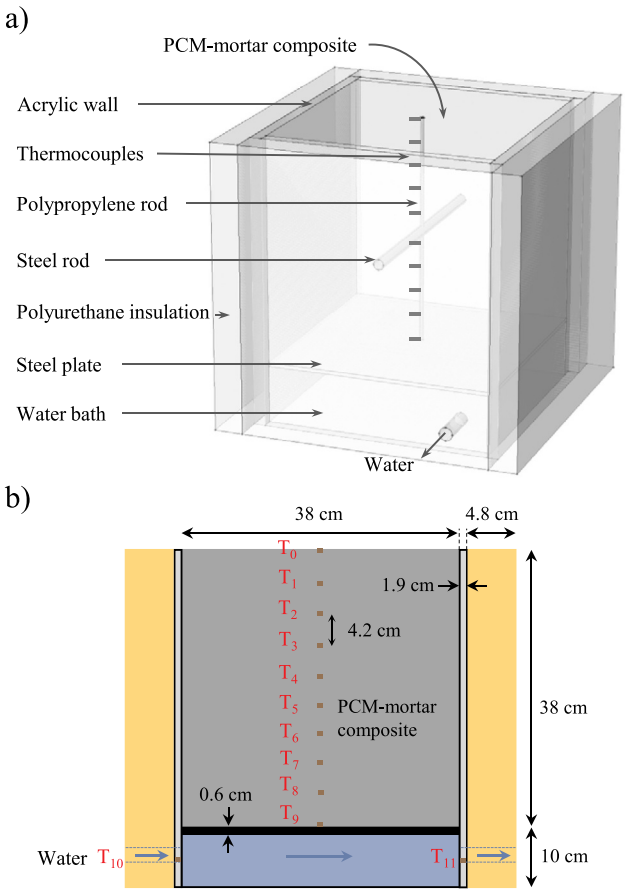

Fig. 1. (a) Schematic of the experimental apparatus with internal dimensions 38 cm × 38 cm × 38 cm. The formwork was made of 1.9 cm thick acrylic while the outside foam was 4.8 cm thick polyurethane. A circulating water bath with dimensions 10 cm × 38 cm × 38 cm was set at the bottom. (b) Sectional view of the experimental apparatus with geometric dimensions.

Table 1
Mixture proportions of the four PCM-mortar composite specimens placed in the experimental apparatus (Fig. 2).

Specimen	Cement paste (vol.%)	ASTM quartz sand (vol.%)	Microencapsulated PCM (vol.%)	Water-cement ratio (%)	WRA (wt.% cement)	VMA 450 (ml/kg of cement)
1	45	55	0	45	0.8	2.6
2	45	45	10 (MPCM24D)	45	1.5	2.6
3	45	45	10 (PCM35CP)	45	1.5	2.6
4	45	35	20 (PCM35CP)	45	2.0	2.6

3.3. Experiments

3.3.1. Experimental test section

Fig. 1a shows a schematic of the experimental test section used to measure transient temperature evolutions within a representative PCM-mortar composite section. The section, in which the different mortars were cast, consisted of a formwork (interior dimensions: 38 cm × 38 cm × 38 cm) with 1.9 cm thick acrylic side walls and 0.6 cm thick stainless steel plate at the bottom. The height of 38 cm (15 inches) was selected to represent the thickness of a pavement section. To reproduce typical environmental conditions, the section was placed in a programmable environmental chamber (TH024, Darwin Chambers Company) where it was subjected to a sinusoidal air temperature profile. In addition, a constant temperature was imposed at the bottom surface of the pavement section by flowing water supplied by a water bath (10 cm × 38 cm × 38 cm) under the stainless steel plate to simulate the constant temperature of the subgrade. Polyurethane foam panels 4.8 cm thick were placed on each vertical side of the box to minimize heat losses.

The temperature at the centerline of the pavement section was measured via 10 type-T thermocouples, denoted by T_0 to T_9, evenly distributed along the vertical direction, as illustrated in Fig. 1. The thermocouples were attached to a vertical polypropylene support (0.8 cm OD, 0.3 cm ID) that was itself supported using a horizontal steel rod (1.8 cm OD, 1.6 cm ID). Both the vertical and horizontal bars were as thin as possible to minimize their effect on the temperature development within the composite sections while still providing sufficient support to maintain the thermocouples in their desired position. The inlet and outlet temperatures of the water bath were monitored by two type-T thermocouples denoted by T_{10} and T_{11}, respectively. The chamber temperature was monitored at four different locations by type-T thermocouples T_{12} to T_{15} to confirm that it was uniform (see supplementary material). All thermocouples were connected to 16-channel input modules (NI 9213, National Instruments) fitted on a compact DAQ chassis (cDAQ-9178, National Instruments). Each input module provided built-in cold-junction compensation. Data acquisition was facilitated by LabVIEW 2014. Fig. 2 shows photographs of the experimental apparatus including (a) thermocouple placement within the test section, (b) inlet and (c) outlet pipes, and (d) the inside of chamber without and (e) with the PCM-mortar composite.

3.3.2. Experimental uncertainty analysis

During each experiment, the temperature of the environmental chamber was controlled within ± 0.2°C, and temperature throughout the chamber was expected to vary by no more than 1°C among different locations. The maximum uncertainty in thermocouple temperature measurements was around ± 0.5°C based on a calibration carried out using a NIST certified refrigerating/heating circulator (AD28R-30-A11B, PolyScience) between 5 and 70°C. The uncertainty in the thermocouple locations was on the order of ± 3 mm, and the corresponding temperature error caused by the uncertainty in location was less than ± 0.2°C based on the numerical simulation results.

3.4. Experimental procedure

The PCM-mortar composites were cast into the cubic acrylic mold shown in Fig. 2. After placement, temperature measurements were recorded as a function of time for 28 days. The water temperature, set to 20°C, was controlled by the refrigerating/heating circulator previously used for thermocouple calibration. The temperature difference between inlet and outlet was less than 1°C throughout the duration of the test (see supplementary material). Thus, the water temperature could be treated as constant.

Each PCM-mortar specimen was placed in the environmental chamber and subjected to sinusoidal temperature cycles with period

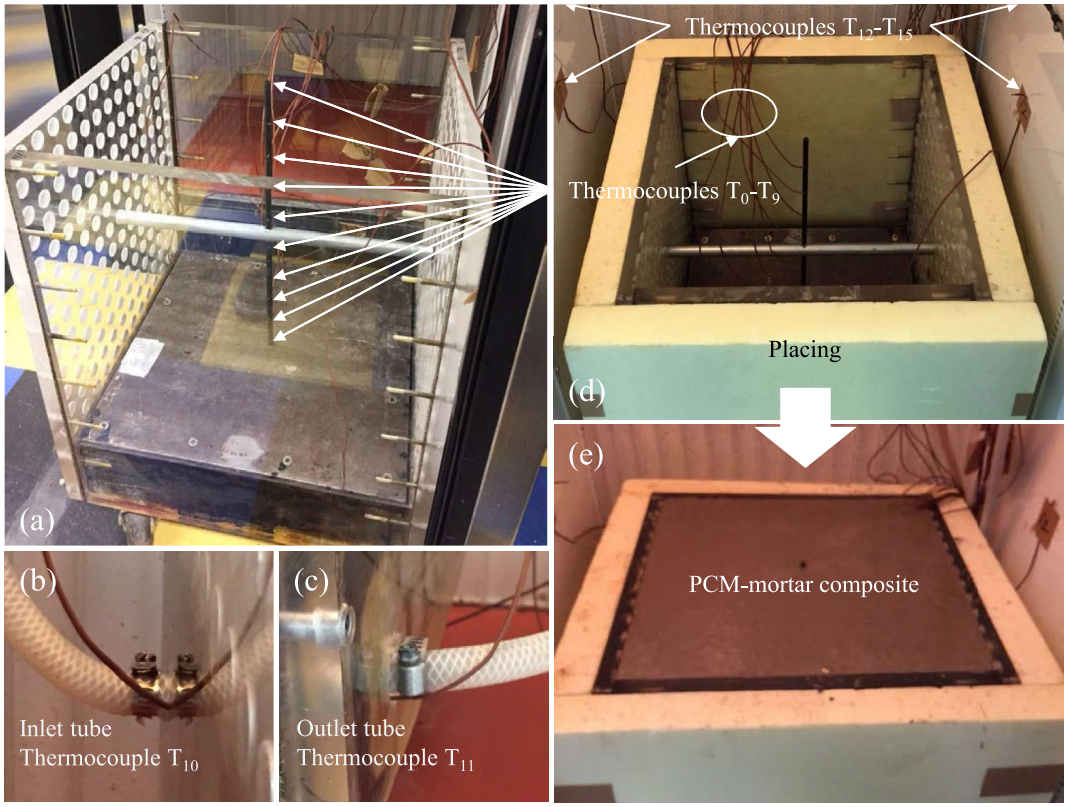

Fig. 2. Photographs of the experimental apparatus and thermocouple placement. (a) Ten thermocouples T_0 - T_9 were evenly placed along a vertical polypropylene rod supported by a horizontal steel rod. Thermocouples T_{10} and T_{11} were inserted into (b) the inlet and (c) the outlet tubes of water bath. (d) Four thermocouples T_{12} - T_{15} were pasted on the inside walls of the environmental chamber. (e) Overview of a PCM-mortar composite specimen placed in experimental apparatus.

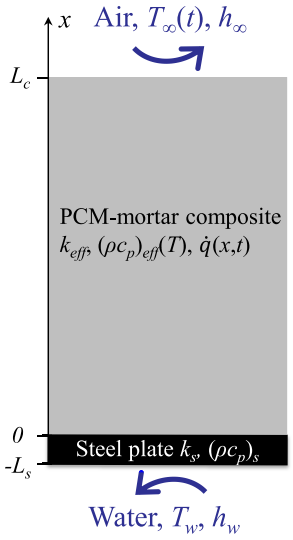

Fig. 3. Schematic of the 1D thermal model of the homogeneous PCM-mortar composite of thickness L_c with effective thermal properties k_{eff} and $(\rho c_p)_{eff}$ placed over a steel plate (k_s and $(\rho c_p)_s$) cooled by water at temperature T_w.

Table 3
Density ρ and specific heat c_p of cement paste, ASTM quartz sand, MPCM24D, and PCM35CP.

Material	Subscript	ρ (kg/m^3)	c_p (J/kg K)	Ref.
Cement paste	m	1965	1530	[39]
ASTM quartz sand	q	2650	745	[30]
MPCM24D	pcm,1	900	$c_{pcm,1}(T)$	[21]
PCM35CP	pcm,2	825	$c_{pcm,2}(T)$	

$\tau = 24$ h with minimum and maximum of 10°C and 40°C, respectively, such that the chamber temperature $T_\infty(t)$ was given by

$$T_\infty(t) = 15 \sin\left(\frac{\pi}{12}t\right) + 25°C \quad (5)$$

where t is in hours.

4. Analysis

4.1. Schematic and assumptions

Fig. 3 illustrates the simulated 1D domain of the experimental test section. The PCM-mortar composite section was treated as homogeneous with effective thermal conductivity k_{eff} and volumetric heat capacity $(\rho c_p)_{eff}(T)$ and subjected to a local heat generation rate per unit volume $\dot{q}(x, t)$. The upper surface of the pavement ($x = L_c$) experienced convective heat transfer with the air in the chamber at temperature $T_\infty(t)$ with convective heat transfer coefficient h_∞. The steel plate below the PCM-mortar composite specimen had a thermal conductivity k_s and volumetric heat capacity $(\rho c_p)_s$. The bottom surface of the steel plate ($x = 0$)experienced convective heat transfer with water at temperature T_w with convective heat transfer coefficient h_w.

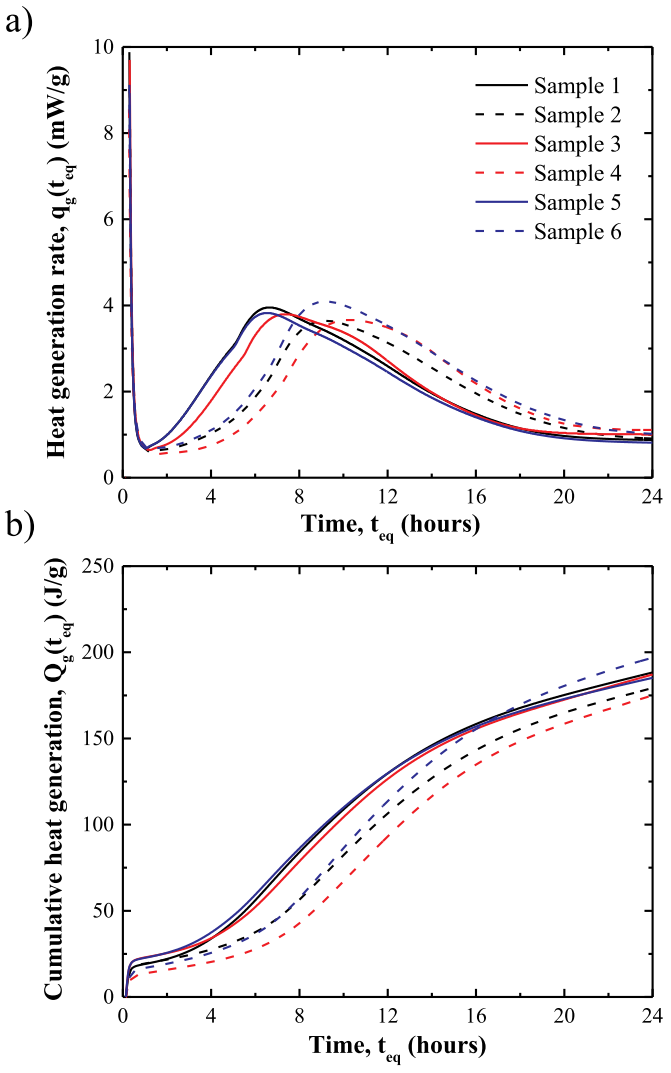

Fig. 4. (a) Experimentally measured isothermal heat generation rate $q_g(t_{eq})$ per unit mass of cement at 25°C for different sample compositions listed in Table 2. (b) Corresponding isothermal thermal energy $Q_g(t_{eq})$ released per unit mass of cement.

The following assumptions were made to make the problem mathematically tractable: (i) the microencapsulated PCM-mortar composite behaved as a homogeneous medium with effective thermal properties k_{eff} and $(\rho c_p)_{eff}(T)$, (ii) all materials were isotropic with constant properties except for the PCM's specific heat capacity which depended on temperature [Eq. (2)], (iii) the convective heat transfer coefficients h_∞ and h_w remained constant, and (iv) evaporative cooling at the specimen surface was negligible.

4.2. Governing equations

The temperature within the PCM-mortar composite section $T_c(x, t)$

Table 4
Effective thermal properties k_{eff} and $(\rho c_p)_{eff}(T)$ of each PCM-mortar composite specimen used in numerical simulation.

Specimen	ϕ_m	ϕ_{pcm}	ϕ_q	k_{eff} (W/m K) [20]	$(\rho c_p)_{eff,s}$ (MJ/m^3 K)	$(\rho c_p)_{eff,high}$ (MJ/m^3 K)
1	0.45	0	0.55	1.77 ± 0.27	2.439	2.439
2	0.45	0.10	0.45	1.46 ± 0.22	2.412	4.212
3	0.45	0.10	0.45	1.46 ± 0.22	2.398	10.11
4	0.45	0.20	0.35	1.27 ± 0.19	2.357	17.78

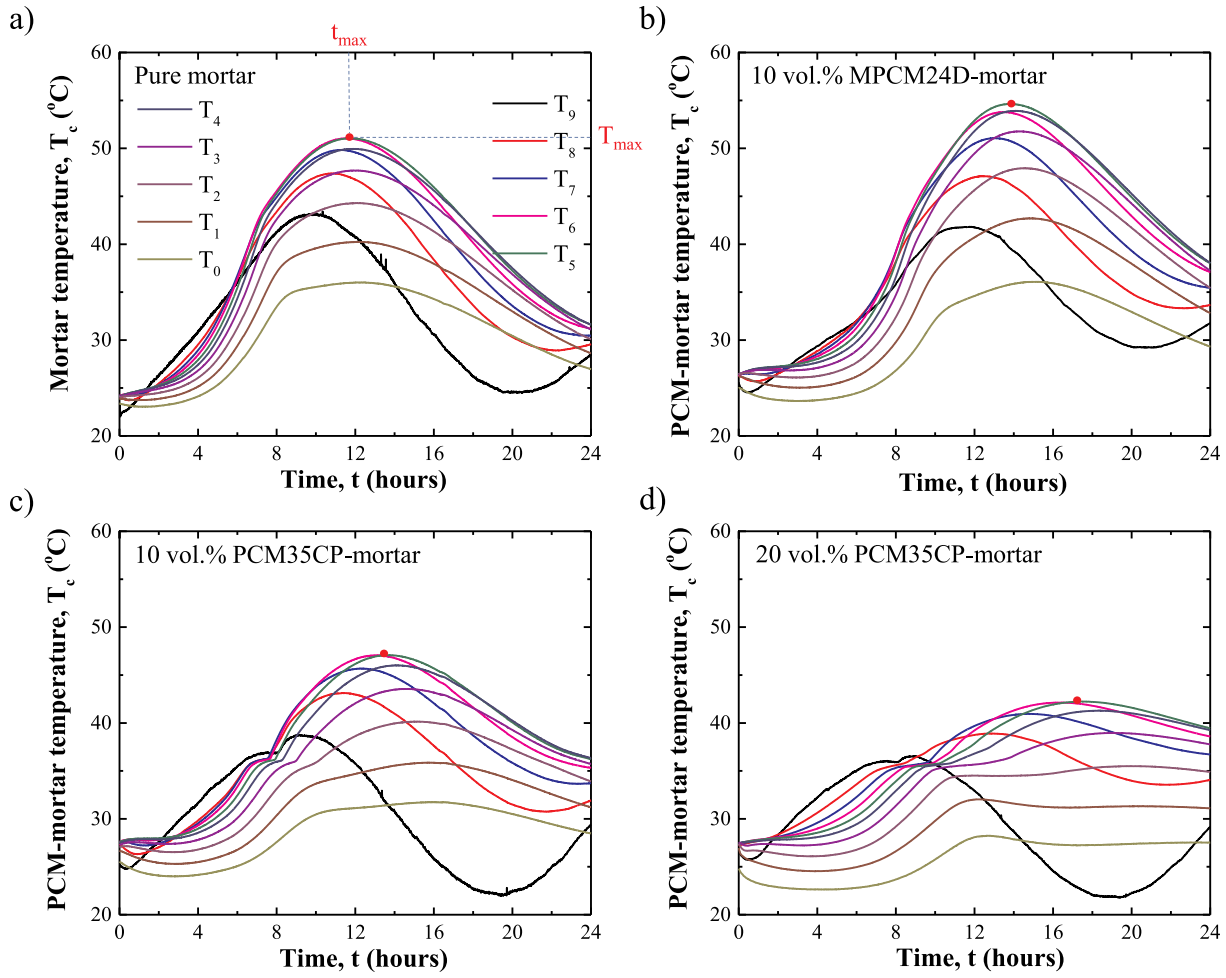

Fig. 5. Experimentally measured temperature as a function of time at ten different locations along the vertical centerline of each PCM-mortar composite specimen during the first 24 h after placement for (a) pure mortar, (b) 10 vol% MPCM24D-mortar composite, (c) 10 vol% PCM35CP-mortar composite, and (d) 20 vol% PCM35CP-mortar composite. See Table 1 for composition.

was governed by the 1D transient heat diffusion equation with heat generation [30], i.e.,

$$(\rho c_p)_{eff}(T_c)\frac{\partial T_c}{\partial t} = k_{eff}\frac{\partial^2 T_c}{\partial x^2} + \dot{q}(x, t). \tag{6}$$

Here, $\dot{q}(x, t)$ is the local heat generation rate per unit volume given by Eq. (4) and expressed in W/m^3. Similarly, the temperature of the steel plate section $T_s(x, t)$ was governed by the 1D transient heat diffusion equation but without heat generation [30],

$$(\rho c_p)_s\frac{\partial T_s}{\partial t} = k_s\frac{\partial^2 T_s}{\partial x^2}. \tag{7}$$

4.3. Initial and boundary conditions

The mixing and placement were conducted at room temperature. Thus, the initial temperature of PCM-mortar composite and steel plate were equal to the room temperature for each case, i.e.,

$$T_c(x, 0) = T_s(x, 0) = T_{room}. \tag{8}$$

To account for the fact that cement hydration was already taking place during the mixing process before placement, the specimen was taken to be at an initial equivalent age of 0.5 h calculated from Equation (3), i.e.,

$$t_{eq}(x, 0) = 0.5 \text{ h}. \tag{9}$$

Convective boundary conditions were applied both on the top surface of the PCM-mortar composite and at the bottom surface of the steel plate and expressed as,

$$-k_{eff}\frac{\partial T_c}{\partial x}\bigg|_{x=L_c} = h_\infty[T_c(L_c, t) - T_\infty(t)] \tag{10}$$

$$-k_s\frac{\partial T_s}{\partial x}\bigg|_{x=-L_s} = h_w[T_w - T_s(-L_s, t)]. \tag{11}$$

Finally, the temperature and heat flux were continuous across the interface of the PCM-mortar composite and the steel plate at all times, i.e.,

$$T_c(0, t) = T_s(0, t) \text{ and } -k_{eff}\frac{\partial T_c}{\partial x}(0, t) = -k_s\frac{\partial T_s}{\partial x}(0, t). \tag{12}$$

4.4. Heat generation

According to Equation (4), the local heat generation rate $\dot{q}(x, t)$ from cement-water reactions at a given location can be expressed in terms of equivalent age $t_{eq}(x, t)$ and of the heat generation rate $\dot{q}(t_{eq})$ obtained from isothermal calorimetry. The latter can be expressed as the product of the cement content C_c (in kg/m^3) and the heat generation rate $\dot{q}_g(t_{eq})$ (in W/kg) per unit mass of cement [i.e., $\dot{q}(t_{eq}) = C_c\dot{q}_g(t_{eq})$], so that

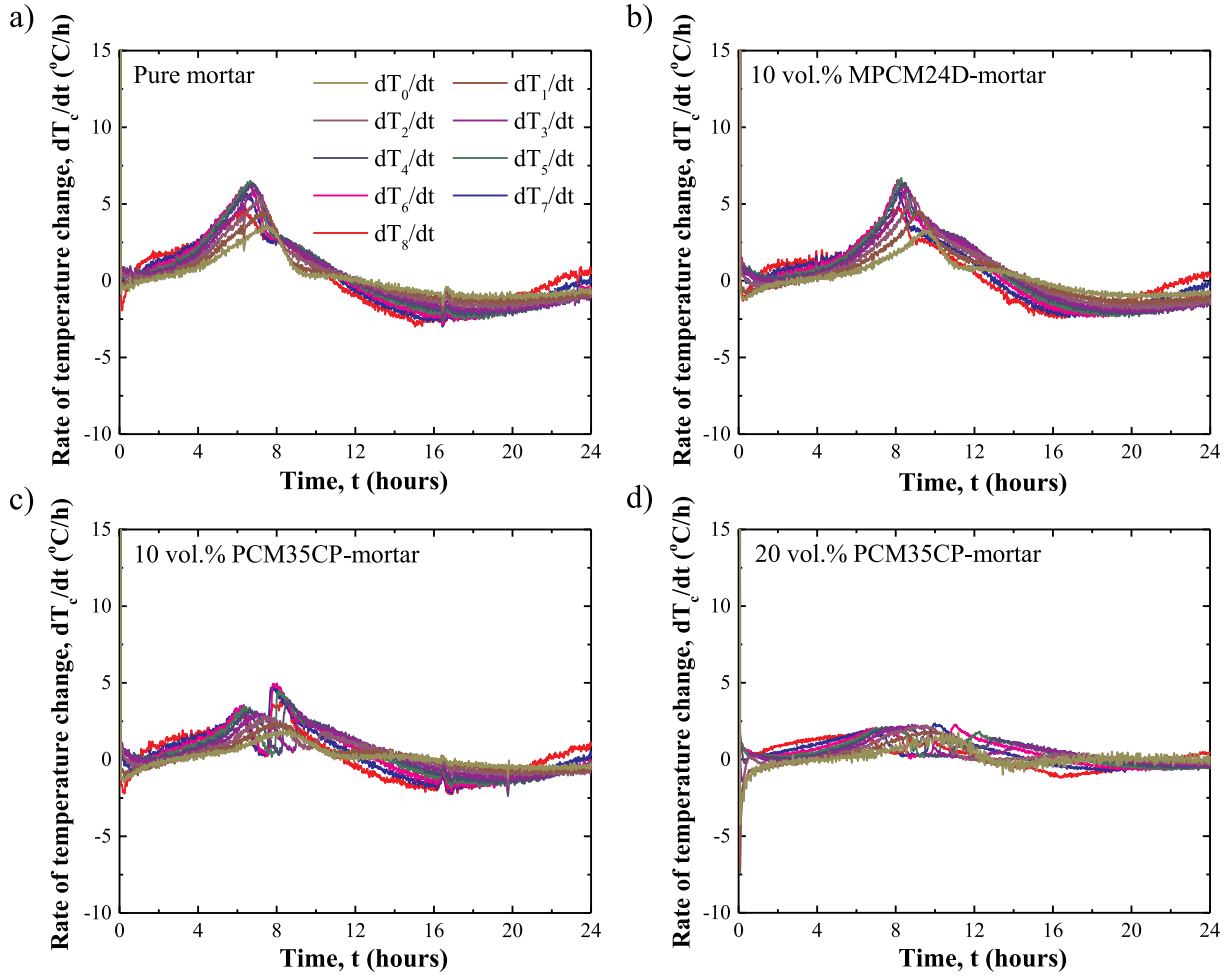

Fig. 6. Experimentally measured rate of temperature change as a function of time at nine different locations along the vertical centerline of each PCM-mortar composite specimen during the first 24 h after placement for (a) pure mortar, (b) 10 vol% MPCM24D-mortar composite, (c) 10 vol% PCM35CP-mortar composite, and (d) 20 vol% PCM35CP-mortar composite. See Table 1 for composition.

$$\dot{q}(x,\,t) = C_c \dot{q}_g(t_{eq}) \exp\left[-\frac{E_a}{R}\left(\frac{1}{T_c(x,\,t)} - \frac{1}{T_{ref}}\right)\right], \tag{13}$$

where E_a ranges between 30 and 60 kJ/mol. Here, the average activation energy for the first 24 h after placement was taken as 31.9 kJ/mol [3].

4.5. Constitutive relationships

Table 3 summarizes the density and specific heat capacity of the cement paste, quartz sand, MPCM24D and PCM35CP used in the numerical simulations. The MPCM24D's latent heat of fusion h_{sf} was 160 kJ/kg with melting temperature T_{pc} = 24°C, and phase change temperature window $\Delta T_{pc} \approx 8$°C [21]. The latent heat of fusion h_{sf} of PCM35CP was 187 kJ/kg with melting temperature T_{pc} = 35°C, and phase change temperature window $\Delta T_{pc} \approx 2$°C. Equation (2) was used to predict the PCM's specific heat capacity as a function of temperature based on $c_{p,pcm,s}$, T_{pc}, ΔT_{pc}, and h_{sf} for each microencapsulated PCM considered. The effective thermal conductivity k_{eff} shown in Table 4 corresponds to that of mortar and MPCM24D-mortar composites aged for 28 days and measured experimentally using the guarded hot-plate method [20]. Here, the mortar and PCM-mortar composite thermal conductivities were assumed to be independent of aging. In addition, because MPCM24D and PCM35CP consisted of similar materials (paraffin core within a melamine-formaldehyde shell), the effective thermal conductivity k_{eff} of PCM35CP-mortar composite was considered to be the same as that of MPCM24D-mortar composite, for given PCM and quartz sand volume fractions.

The water bath temperature T_w was taken as the measured time-averaged constant temperature $T_w = (T_{10} + T_{11})/2 \approx 20.3$°C. The initial temperature of the composite $T_c(x, 0)$ and steel plate $T_s(x, 0)$ were taken as room temperature T_{room} equal to about 25°C.

Finally, after 28 days, cement-water reactions diminished sufficiently that heat generation was no longer significant. Hence, the temperature evolution within the mortar section reached a periodic steady state. Then, the convective heat transfer coefficients h_∞ at the top surface of the composite and h_w at the bottom surface of the steel plate were evaluated by least square fitting of the measured periodic steady state temperature $T_{exp}(x_j, t_i)$ and the predicted periodic steady state temperature $T_c(x_j, t_i)$ of the composite section on the 30th day. The objective function was expressed as,

$$f(h_\infty, h_w) = \sum_{j=1}^{N_T} \sum_{i=1}^{N_t} \left[T_{\exp}(x_j, t_i) - T_c(x_j, t_i)\right]^2 \tag{14}$$

where $j \in [1, N_T]$ corresponds to each of the N_T = 10 thermocouples, while $i \in [1, N_t]$ corresponds to the temporal measurements acquired during N_t = 2880 time steps every 30 s during the course of one day of experiment. The convective heat transfer coefficients were estimated to be h_∞ = 25 W/m^2 K and h_w = 18 W/m^2 K.

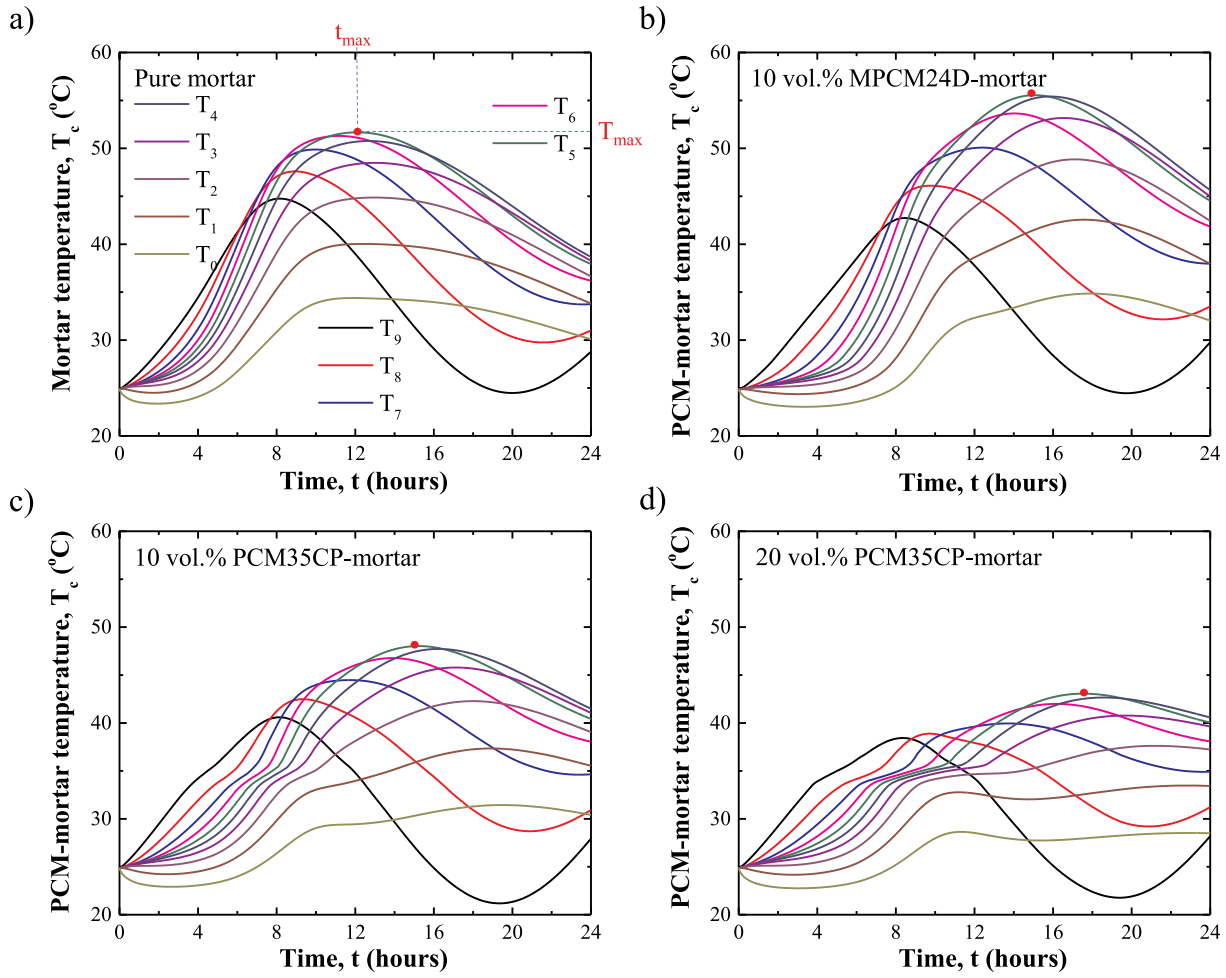

Fig. 7. Numerically predicted temperature as a function of time at ten different locations along the vertical centerline of each PCM-mortar composite specimen during the first 24 h after placement for (a) pure mortar, (b) 10 vol% MPCM24D-mortar composite, (c) 10 vol% PCM35CP-mortar composite, and (d) 20 vol% PCM35CP-mortar composite. See Table 1 for composition.

4.6. Method of solution

The transient 1D governing Equations (6) and (7) for $T_c(x, t)$ and $T_s(x, t)$ were solved along with the corresponding boundary and initial conditions Equations (8)–(12) using a semi-implicit finite difference method [30]. The solution was considered to be numerically converged when the resulting composite temperature $T_c(x, t)$ at any time t or spatial location x differed by no more than 1% after reducing the nodal spacing Δx and the time step Δt by a factor of 2. A nodal spacing $\Delta x = 3$ mm and time step $\Delta t = 30$ s were sufficient to achieve a numerically converged solution.

5. Results and discussion

5.1. Effect of inclusions and admixtures on hydration

To assess the effect of PCM, quartz sand inclusions, and water-reducing admixture (WRA) on cement hydration, isothermal calorimetry measurements of heat generation rates $\dot{q}_g(t)$ in mortar samples with compositions summarized in Table 2 were carried out at $T_{ref} = 25$°C. Fig. 4a shows the measured heat generation rate $\dot{q}_g(t_{eq})$ for the six different mortar compositions. Fig. 4b shows the corresponding measured total thermal energy $Q_g(t_{eq})$ in (J/g) released during cement hydration and expressed as

$$Q_g(t_{eq}) = \int_0^{t_{eq}} \dot{q}_g(t_{eq}) \mathrm{d}t_{eq}. \quad (15)$$

It is evident that the PCM and quartz inclusions had no significant influence on $\dot{q}_g(t_{eq})$ and $Q_g(t_{eq})$. However, the addition of WRA delayed the heat generation peak from 6 h to 9 h and decreased the total thermal energy $Q_g(t_{eq})$ released in the first 12 h in order of increasing WRA dosage. These results were consistent with previous studies [31,32].

5.2. Experimental temperature profiles of PCM-mortar composites

Fig. 5 plots the temporal evolution of local composite temperature $T_c(x, t)$ at various spatial locations from the bottom ($x = 0$) to the top ($x = L_c$) of the four PCM-mortar specimens with compositions summarized in Table 1. The maximum temperature was always reached near the middle of the test section around 12–17 h after placement. Fig. 5b establishes that adding 10 vol% MPCM24D into the mortar did not reduce its early-age temperature compared with the plain mortar section (Fig. 5a). Instead, the temperature rise was delayed from around 12 h to around 14 h after placement and the maximum temperature increased from 51°C to 54°C. These observations could be attributed to the fact that (i) the WRA added to the formulation retarded the rates of hydration reactions and (ii) the effective thermal conductivity of the composite decreased as MPCM24D was added thus preventing heat dissipation to the surroundings. Note also that the PCM's latent heat was not exploited because the MPCM24D had already melted prior to the start of the experiment, i.e., since the initial temperature of the mortar was around 25°C (Fig. 5b). However, Fig. 5c indicates that adding 10 vol% PCM35CP reduced the maximum temperature from

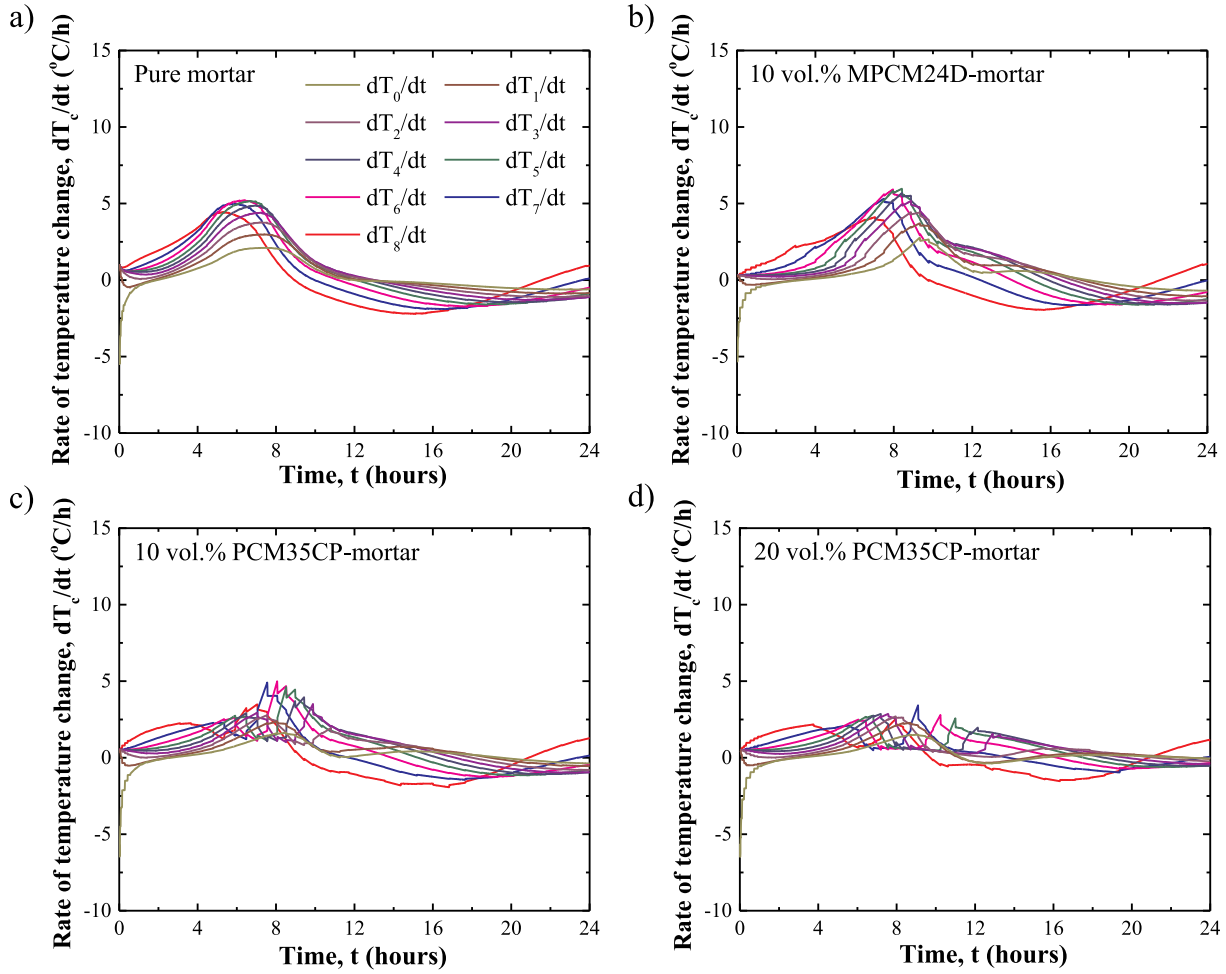

Fig. 8. Numerically predicted rate of temperature change as a function of time at nine different locations along the vertical centerline of each PCM-mortar composite specimen during the first 24 h after placement for (a) pure mortar, (b) 10 vol% MPCM24D-mortar composite, (c) 10 vol% PCM35CP-mortar composite, and (d) 20 vol % PCM35CP-mortar composite. See Table 1 for composition.

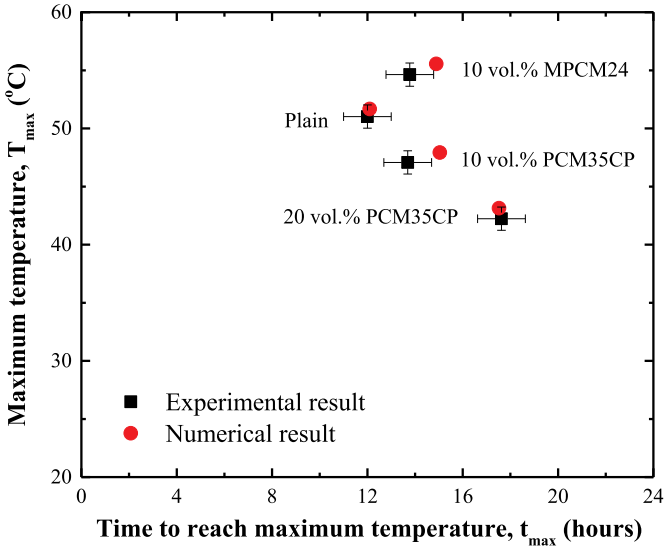

Fig. 9. Comparison of experimentally measured and numerically predicted maximum temperature T_{max} and corresponding time t_{max} within the PCM-mortar composite sections during the first 24 h after placement.

51°C to 47°C. The temperature evolution also plateaued after around 8 h at around 35°C due to the melting of the PCM. Finally, Fig. 5d established that adding 20 vol% PCM35CP further reduced the maximum temperature to 42°C and delayed the temperature peak further to around 17 h; although this delay is attributable to the increased WRA dosage. Nevertheless, the results indicate that dosage of PCMs with phase change temperature of 35°C can reduce temperature rise in cementitious formulations by nearly 10°C, thereby reducing the risk of early-age thermal cracking.

5.3. Experimental rate of temperature change in PCM-mortar composites

Fig. 6 plots the local rate of temperature change at different spatial locations from the bottom ($x = 0$) to near the top ($x = 8L_c/9$) for (a) pure mortar, (b) 10 vol% MPCM24D-mortar composite, (c) 10 vol% PCM35CP-mortar composite, and (d) 20 vol% PCM35CP-mortar composite (Table 1). Note that the local rate of temperature change dT_9/dt measured on the top surface ($x = L_c$) was not shown because it fluctuated substantially and unrealistically over time as it was measured near the air/PCM-mortar interface. The highest rate of temperature change was systematically reached near the middle of the test section around 6–10 h after placement. The lowest rate of temperature change ($dT_c/dt < 0$), which corresponded to the highest cool-down rate, was always reached near the top surface of the test sections about 14 h after placement where cooling was the strongest. The cool-down rate decreased when the location of measurement was closer to the bottom

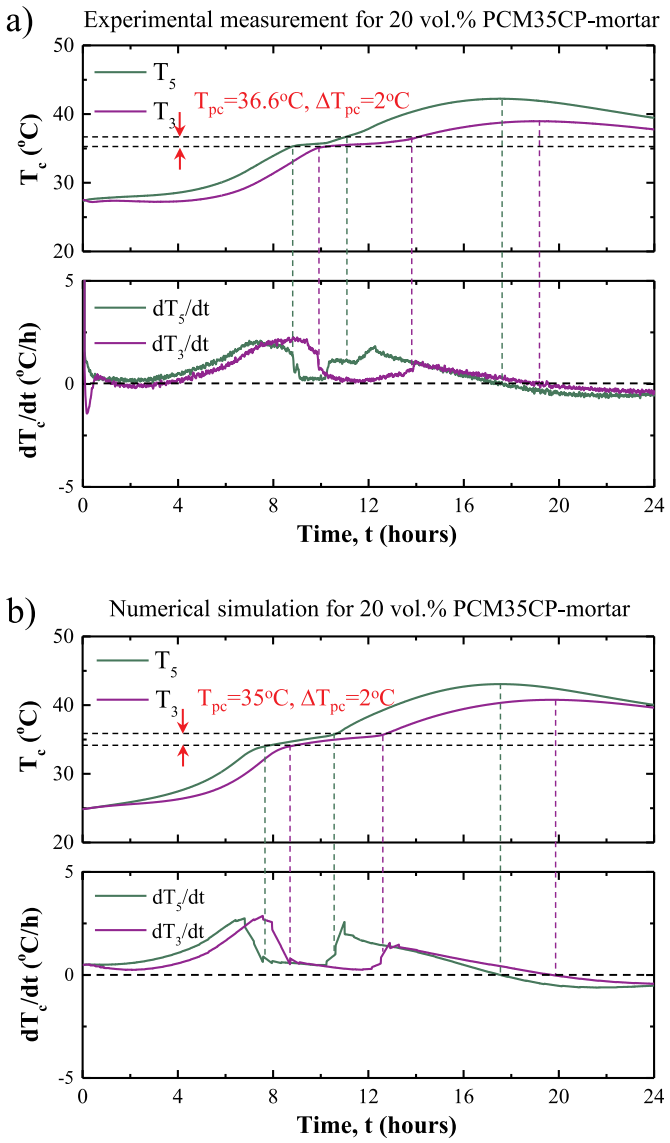

Fig. 10. (a) Experimentally measured and (b) numerically predicted temperature and corresponding rate of temperature change as functions of time at $3L_c/9$ and $5L_c/9$ of 20 vol% PCM35CP-mortar composite.

surface. Fig. 6c and 6d establish that adding PCM35CP reduced both temperature rise rate and the cool-down rate within PCM-mortar composite section in the first 24 h after placement except near the top surface. This effect was stronger with increasing PCM loading. These results establish that adding PCM with proper phase change temperature and dosage can reduce the cool-down rate of PCM-mortar composite considerably thus reducing both the risk of early-age cracking due to shrinkage and the depth of crack [16].

5.4. Comparison between experiments and numerical simulations

Figs. 7 and 8 respectively show the numerically simulated temporal evolution of temperature and the corresponding rate of temperature change along the centerline of the pavement section at the same set of locations as in the experiments. Comparison with experimental results shown in Figs. 5 and 6 indicate that numerical simulations agree very well qualitatively and quantitatively with experimental data. For example, the numerically predicted maximum temperature and highest rate of temperature change were reached near the middle of the test section at the same time as that observed experimentally. In addition, Fig. 9 compares the experimentally measured and numerically predicted maximum temperature T_{max} versus the corresponding time t_{max} for the four PCM-mortar composite specimens of interest (Table 1). The experimental uncertainty in the maximum temperature T_{max} was ± 1°C and the corresponding uncertainty in t_{max} was around ± 1 h. Fig. 9 shows good agreement between experimental measurements and numerical predictions for both T_{max} and t_{max}. The discrepancies were likely caused by the uncertainties in the effective thermal properties k_{eff} and $(\rho c_p)_{eff}$ used in the simulations.

Fig. 10 shows (a) the experimental measurements and (b) the numerical predictions of the local temperature T_3 at $x = 3L_c/9$ and T_5 at $x = 5L_c/9$ and the corresponding rates of temperature change dT_3/dt and dT_5/dt for 20 vol% PCM35CP-mortar composite. Both plots feature a common plateau after around 8 h when temperature approached the PCM melting temperature of 35°C. In other words, dT_c/dt approached 0 when PCM was melting in the temperature range $T_{pc} \pm \Delta T_{pc}/2$. Consequently PCM melting helped reduce the temperature rise and damp the rate of temperature change of concrete at early ages. Overall, the 1D transient thermal model developed performed well and can be used to accurately predict temperature development and cool-down rate within early-age concrete pavements.

6. Implications of the dosage of phase change materials on thermal cracking risks

The additions of microencapsulated PCMs has been shown to reduce the compressive and flexural strength of the resulting cement-based composite [33–36]. However, for a useful range of dosage, the strength remains sufficiently high for many practical applications [34]. In addition, some of the undesirable mechanical effects can be compensated by the simultaneous dosage of stiff inclusions [37]. Nevertheless, in spite of a drop in compressive strength, the tensile strength remains nearly unchanged [7,34–37], while the cracking risk in fact decreases due to the contributions of improved stress relaxation and cracking blunting/deflection [38]. The outcomes of this study highlight that microencapsulated phase change materials, when suitably chosen and dosed, are effective at reducing both maximum temperature rise T_{max} and the cool-down rate $|dT_c/dt|$ of concrete pavement sections. Given the dominant role of these two variables on affecting cracking risks, it is clear that any suppression of T_{max} and $|dT_c/dt|$ would result in correlated reductions in the thermal cracking risk, as demonstrated in the literature [7,14,35]. This is also borne out by analysis of the vertical temperature gradient that develops in sections containing PCMs wherein a shallower temperature gradient develops from the pavement surface to the subgrade. Such a reduction in the temperature (strain) gradient is yet another important consideration in reducing the risk of cracking [3]. The outcomes of this work gain greater significance when the impacts of PCM additions, i.e., as a soft inclusion are considered. Specifically, due to their ability to enhance stress relaxation, and ensure crack blunting and deflection [38], microencapsulated PCMs offer two routes, i.e., based on temperature control, and mechanical effects in reducing the cracking risk of restrained concrete elements. These attributes are especially beneficial in the case of horizontal elements such as pavements, and bridge-decks which feature substantial exposure to both early- and later-age temperature variations.

7. Conclusion

This study has demonstrated the ability of PCM dosages in reducing both the maximum temperature developed and the cool-down rate of realistic concrete pavement geometries over the first 24 h after placement. However, this requires the dosage of microencapsulated PCMs that feature a melting temperature above the placement temperature. A 1D transient thermal model was also developed using the heat generation rate measured by isothermal calorimetry based on the time-temperature equivalent age method. Good qualitative and quantitative

agreements were observed between experimentally measured and numerically predicted temperature evolutions within the different mortar sections. Thus, the 1D thermal model with the thermophysical properties of PCM-mortar composite and heat generation rate associated with cement hydration can be used to predict temperature evolutions, and thereby estimate the risk of cracking in pavements, and other restrained concrete elements.

Acknowledgements

The authors acknowledge financial support for this research provided by an Infravation ERA-NET Plus Grant (31109806.0001: ECLIPS) and the University of California, Los Angeles (UCLA). The contents of this paper reflect the views and opinions of the authors, who are responsible for the accuracy of the datasets presented herein, and not necessarily the views of the funding organizations. The Laboratory for the Chemistry of Construction Materials (LC^2) at the University of California, Los Angeles (UCLA) acknowledges the support that has made its operations possible.

Appendix A. Supplementary data

Supplementary data to this article can be found online at https://doi.org/10.1016/j.cemconcomp.2019.04.002.

References

[1] D.P. Bentz, A review of early-age properties of cement-based materials, Cement Concr. Res. 38 (2) (2008) 196–204.
[2] B. Zhu, Thermal Stresses and Temperature Control of Mass Concrete, Butterworth-Heinemann, Oxford, UK, 2013.
[3] B.A. Young, G. Falzone, Z. She, A.M. Thiele, Z. Wei, N. Neithalath, G. Sant, L. Pilon, Early-age temperature evolutions in concrete pavements containing micro-encapsulated phase change materials, Constr. Build. Mater. 147 (2017) 466–477.
[4] S.N. AL-Saadi, Z.J. Zhai, Modeling phase change materials embedded in building enclosure: a review, Renew. Sustain. Energy Rev. 21 (2013) 659–673.
[5] K.L. Lees and K.R. Edwars. Cryogenic cooling of concrete, June 8, 1971. US Patent 3,583,172.
[6] D.P. Bentz, R. Turpin, Potential applications of phase change materials in concrete technology, Cement Concr. Compos. 29 (7) (2007) 527–532.
[7] F. Fernandes, S. Manari, M. Aguayo, K. Santos, T. Oey, Z. Wei, G. Falzone, N. Neithalath, G. Sant, On the feasibility of using phase change materials (PCMs) to mitigate thermal cracking in cementitious materials, Cement Concr. Compos. 51 (2014) 14–26.
[8] C. Qian, G. Gao, C. Zhu, Z. Guo, Influence of phase change materials on temperature rise caused by hydration heat evolution of cement-based materials, Mag. Concr. Res. 62 (11) (2010) 789–794.
[9] C. Qian, G. Gao, Reduction of interior temperature of mass concrete using suspension of phase change materials as cooling fluid, Constr. Build. Mater. 26 (1) (2012) 527–531.
[10] V.V. Tyagi, D. Buddhi, PCM thermal storage in buildings: a state of art, Renew. Sustain. Energy Rev. 11 (6) (2007) 1146–1166.
[11] L.F. Cabeza, C. Castellon, M. Nogues, M. Medrano, R. Leppers, O. Zubillaga, Use of microencapsulated PCM in concrete walls for energy savings, Energy Build. 39 (2) (2007) 113–119.
[12] A. Jamekhorshid, S.M. Sadrameli, M. Farid, A review of microencapsulation methods of phase change materials (PCMs) as a thermal energy storage (TES) medium, Renew. Sustain. Energy Rev. 31 (2014) 531–542.
[13] G. Fang, Z. Chen, H. Li, Synthesis and properties of microencapsulated paraffin composites with SiO_2 shell as thermal energy storage materials, Chem. Eng. J. 163 (1) (2010) 154–159.
[14] A. Arora, G. Sant, N. Neithalath, Numerical simulations to quantify the influence of phase change materials (PCMs) on the early-and later-age thermal response of concrete pavements, Cement Concr. Compos. 81 (2017) 11–24.
[15] B. Šavija, E. Schlangen, Use of phase change materials (PCMs) to mitigate early age thermal cracking in concrete: theoretical considerations, Constr. Build. Mater. 126 (2016) 332–344.
[16] B. Klemczak, A. Knoppik-Wróbel, Early age thermal and shrinkage cracks in concrete structures–description of the problem, Archit. Civil Eng. Environ. 4 (2) (2011) 35–48.
[17] A.M. Thiele, A. Kumar, G. Sant, L. Pilon, Effective thermal conductivity of three-component composites containing spherical capsules, Int. J. Heat Mass Transf. 73 (2014) 177–185.
[18] A.M. Thiele, G. Sant, L. Pilon, Diurnal thermal analysis of microencapsulated PCM-concrete composite walls, Energy Convers. Manag. 93 (2015) 215–227.
[19] J.D. Felske, Effective thermal conductivity of composite spheres in a continuous medium with contact resistance, Int. J. Heat Mass Transf. 47 (14) (2004) 3453–3461.
[20] A. Ricklefs, A.M. Thiele, G. Falzone, G. Sant, L. Pilon, Thermal conductivity of cementitious composites containing microencapsulated phase change materials, Int. J. Heat Mass Transf. 104 (2017) 71–82.
[21] A.M. Thiele, Z. Wei, G. Falzone, B.A. Young, N. Neithalath, G. Sant, L. Pilon, Figure of merit for the thermal performance of cementitious composites containing phase change materials, Cement Concr. Compos. 65 (2016) 214–226.
[22] Z. Ge, K. Wang, Z. Gao, Prediction of pavement concrete strength development, joint sawing, and opening time using FEMLAB, J. Perform. Constr. Facil. 26 (2) (2011) 162–169.
[23] R.C. Tank, N.J. Carino, Rate constant functions for strength development of concrete, Mater. J. 88 (1) (1991) 74–83.
[24] P.F. Hansen, E.J. Pedersen, Maturity computer for controlled curing and hardening of concrete, Nord. Betong 1 (1977) 19–34.
[25] ASTM Standard. C150/C150M-17 Standard Specification for Portland Cement, ASTM International, West Conshohocken, PA, 2017.
[26] ASTM Standard, C192/C192M-16a Standard Practice for Making and Curing Concrete Test Specimens in the Laboratory, ASTM International, West Conshohocken, PA, 2016.
[27] ASTM Standard, C778-13 Standard Specification for Standard Sand, ASTM International, West Conshohocken, PA, 2013.
[28] ASTM Standard, C1702 Standard Test Method for Measurement of Heat of Hydration of Hydraulic Cementitious Materials Using Isothermal Conduction Calorimetry, ASTM International, West Conshohocken, PA, 2015.
[29] ASTM Standard, C494/C494M-17 Standard Specification for Chemical Admixtures for Concrete, ASTM International, West Conshohocken, PA, 2017.
[30] T.L. Bergman, A.S. Lavine, F.P. Incropera, D.P. DeWitt, Fundamentals of Heat and Mass Transfer, seventh ed., John Wiley & Sons, New York, NY, 2011.
[31] A. Jayalath, R. San Nicolas, M. Sofi, R. Shanks, T. Ngo, L. Aye, P. Mendis, Properties of cementitious mortar and concrete containing micro-encapsulated phase change materials, Constr. Build. Mater. 120 (2016) 408–417.
[32] F. Puertas, H. Santos, M. Palacios, S. Martínez-Ramírez, Polycarboxylate superplasticiser admixtures: effect on hydration, microstructure and rheological behaviour in cement pastes, Adv. Cem. Res. 17 (2) (2005) 77–89.
[33] P.K. Dehdezi, M.R. Hall, A.R. Dawson, S.P. Casey, Thermal, mechanical and microstructural analysis of concrete containing microencapsulated phase change materials, Int. J. Pavement Eng. 14 (5) (2013) 449–462.
[34] D. Snoeck, B. Priem, P. Dubruel, N. De Belie, Encapsulated phase-change materials as additives in cementitious materials to promote thermal comfort in concrete constructions, Mater. Struct. 49 (1–2) (2016) 225–239.
[35] B. Šavija, H. Zhang, E. Schlangen, Influence of microencapsulated phase change material (PCM) addition on (micro) mechanical properties of cement paste, Materials 10 (8) (2017) 863.
[36] B. Šavija, Smart crack control in concrete through use of phase change materials (PCMs): a review, Materials 11 (5) (2018) 654.
[37] G. Falzone, G. Puerta Falla, Z. Wei, M. Zhao, A. Kumar, M. Bauchy, N. Neithalath, L. Pilon, G. Sant, The influences of soft and stiff inclusions on the mechanical properties of cementitious composites, Cement Concr. Compos. 71 (2016) 153–165.
[38] Z. Wei, G. Falzone, S. Das, N. Saklani, Y. Le Pape, L. Pilon, N. Neithalath, G. Sant, Restrained shrinkage cracking of cementitious composites containing soft PCM inclusions: a paste (matrix) controlled response, Mater. Des. 132 (2017) 367–374.
[39] D.P. Bentz, Transient plane source measurements of the thermal properties of hydrating cement pastes, Mater. Struct. 40 (10) (2007) 1073–1080.